

Article

Ultrasonic-Assisted Michael Addition of Arylhalide to Activated Olefins Utilizing Nanosized CoMgAl-Layered Double Hydroxide Catalysts

Nada S. Althabaiti ¹, Fawzia M. Al-Nwaiser ¹, Tamer S. Saleh ² and Mohamed Mokhtar ^{1,*} 

¹ Chemistry Department, Faculty of Science, King Abdulaziz University, Jeddah 21589, Saudi Arabia; nadoosh-72@hotmail.com (N.S.A.); falnowaiser@kau.edu.sa (F.M.A.-N.)

² Chemistry Department, Faculty of Science, University of Jeddah, P.O. Box 80329, Jeddah 21589, Saudi Arabia; tamsaid@yahoo.com

* Correspondence: mmoustafa@kau.edu.sa; Tel.: +966-500558045

Received: 27 December 2019; Accepted: 8 February 2020; Published: 11 February 2020



Abstract: An efficient cobalt-based layered double hydroxide (LDH)-catalyzed Michael addition of an aryl halide compound onto activated olefin as a Michael acceptor is described. The synthesized catalytic materials were characterized using different techniques to investigate their physicochemical, morphological, and textural properties. The partial isomorphous substitution of magnesium by cobalt ions in the cationic sheets of the layered double hydroxide (CoMgAl-LDH) appears to be an appropriate catalyst to cause this reaction. This technique enables compound synthesis resulting from the 1,4-addition in good to excellent yields. Moreover, ultrasound was found to have beneficial effect on this reaction due to the cavitation phenomenon.

Keywords: Michael addition; cobalt-based LDHs; ultrasonic irradiation; synergistic effect

1. Introduction

The new formation of carbon–carbon bonds using the conjugate addition of functionalized aryl compounds to Michael acceptors is considered a key point for synthesizing useful organic models for further transformation [1]. Researchers around the world made great efforts to develop new methods of synthesizing this critical reaction for more stable and adaptable problems [2]. Different organometallic catalysts were applied for the regioselective 1,4-addition of aryl halides [3–5]. For these types of reactions, several classical methods were applied, including the use of homogeneous catalysis with palladium salts [6,7], rhodium complexes [8,9], and copper salts [10,11]. Additional transition-metal conjugate additions of major groups of organometallic reagents such as aryl-aluminum, -tin, -silicon, -titanium, -indium, and -boron compounds were also documented [12]. However, these compounds are moisture-sensitive under classical working conditions in air/moisture atmosphere. A direct activation of the aryl halides using chemical and electrochemical processes was developed to avoid such difficulties. On the other hand, homogeneous catalysis remains of highest interest utilizing in situ reduction of transition-metal complexes [13]. The direct electrochemical arylation of electron-deficient olefins carried out utilizing cobalt catalysts in the presence of a sacrificial anode was successful for the synthesis of various aromatic halides [14]. In addition to the difficulties of handling the electrochemical approaches in assessment of the classical ones, the cobalt-based catalyst, CoBr₂, is only effective for electrochemical addition of aryl bromides attached with electron-withdrawing groups. Muriel et al. developed a direct chemical procedure for the conjugate addition of different substituted aryl bromides, chlorides, and triflates, bearing an electron-withdrawing or -donating group, on various activated olefins [15]. Although this one-step chemical process was novel and solved the

problems of pre-preparation of organometallic reagents, using $\text{CoBr}_2(2,2'\text{-bipyridine})$ as a catalyst, it suffered from separation and regeneration difficulties of the selected designed catalysts. A “green” alternative to such reactions that provides high yields and good selectivity with waste reduction can be achieved by using cobalt-based solid heterogeneous catalysts [16].

Layered double hydroxide-based materials (LDHs) exhibit great potential as heterogeneous catalysts due to their versatility, defined by the combination of different catalytically active transition-metal species (e.g., Cu, Co, Fe, Ni, V, Rh), robust alkaline nature, and relaxed product departure [17–19]. Our group of research succeeded in synthesizing many organic synthons via carbon–carbon coupling reactions using LDH-based catalysts [20–22].

In addition, sonochemical synthesis is an important synthesis technique. Unlike traditional methods, this procedure has certain advantages, such as simplicity, short reaction time, controllability, convenience, and good product yields [23–27].

To the best of our knowledge, few reports dealt with a heterogeneous catalyst system for this 1,4-conjugate addition [28–30]. Bearing in mind all of the abovementioned factors, we continued our interest in introducing a benign protocol for organic reactions utilizing heterogeneous catalysts [20,31–34]. We introduce here a facile sonochemical synthesis for the conjugate addition of aryl halides onto electron-deficient olefins utilizing a CoMgAl LDH.

2. Results

2.1. Fourier-Transform Infrared Spectroscopy (FTIR)

FTIR spectra of all the solid materials investigated (Figure 1) showed a 3484 cm^{-1} wide band assigned to the O–H stretching vibration, credited to interlayer water and hydroxyl groups in the layered double hydroxide. The OH stretching modes of weak hydrogen bonds occurred in the area between 3600 and 3500 cm^{-1} for water adsorbed on clay minerals. The OH stretching vibrations and a stretching vibration of interlayer water were due to a broad band about $3300\text{--}3000\text{ cm}^{-1}$ with a shoulder, often apparent, containing two or three overlapping bands. A low peak in the infrared spectrum of around 1630 cm^{-1} was due to the interlayer water mode of $\nu\text{ H}_2\text{O}$. A low peak in the infrared spectrum of around 1630 cm^{-1} was due to the interlayer water mode of $\nu\text{ H}_2\text{O}$. Due to the interaction of carbonate with interlayer water molecules and/or hydroxyl groups from the Mg–Al LDH base, the integration of the carbonate species into the layered structure showed a change toward lower wave numbers. Layered double carbonate hydroxides typically show infrared bands at about $1360\text{--}1400$, 875 , and 670 cm^{-1} , which are generally absent from the given spectrum in the interlayer. The obtained results indicate that a pure layered double hydroxide with hydroxyl groups and water molecules in the interlayer gallery was synthesized using the hydrothermal post-treated coprecipitation method.

The spectra of the CoMgAl-LDH and CoAl-LDH samples revealed bands below 1000 cm^{-1} as a result of stretching/deformation modes of the M–O, M–O–M, and O–M–O layers [35]. The peak at 620 cm^{-1} could be attributed to the existence of Co^{II} and Co–OH conversion, while the signal at 565 cm^{-1} remained due to the Al–OH translational mode [36].

2.2. Thermal Gravimetric Analysis (TGA)

Thermal gravimetric analysis was conducted for all of the catalysts investigated (Figure 2). For the MgAl-LDH study, four significant mass loss measures could be identified: (a) a poor mass loss at $50\text{--}140\text{ }^\circ\text{C}$ with a shoulder at $132\text{ }^\circ\text{C}$ owing to the loss of physisorbed water; (b) a strong mass loss signal at $135\text{--}300\text{ }^\circ\text{C}$ at a height of $222\text{ }^\circ\text{C}$, primarily due to the loss of understructure losses [37–39]; (c) a large mass loss between 250 and $600\text{ }^\circ\text{C}$ (maximum at 330 , 352 , and $410\text{ }^\circ\text{C}$) due to the evolution of H_2O vapor, which confirmed the process of dehydroxylation of the brucite structure by dihydroxylation; (d) one last mass loss at $499\text{ }^\circ\text{C}$ for the decomposition of metal hydroxides, leading to the formation of metal oxides.

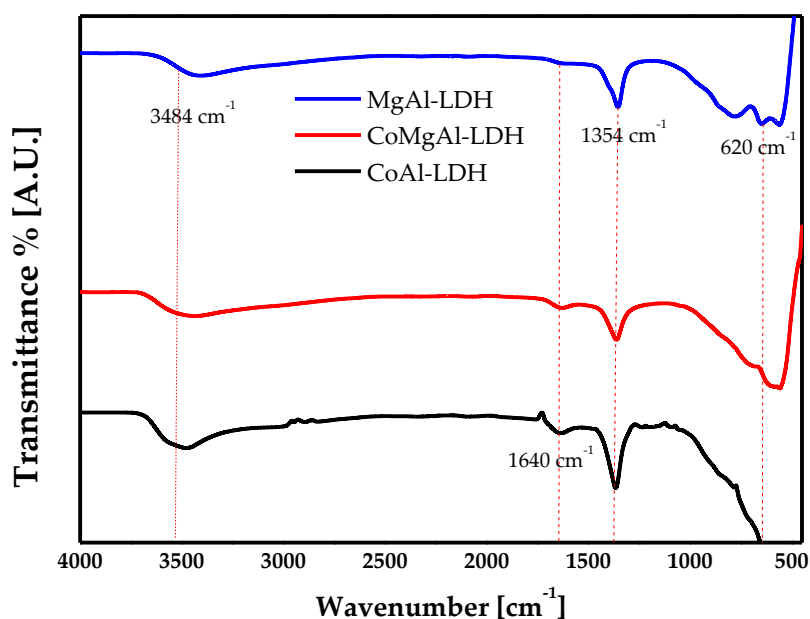


Figure 1. Fourier-transform infrared (FTIR) spectra of all the investigated samples.

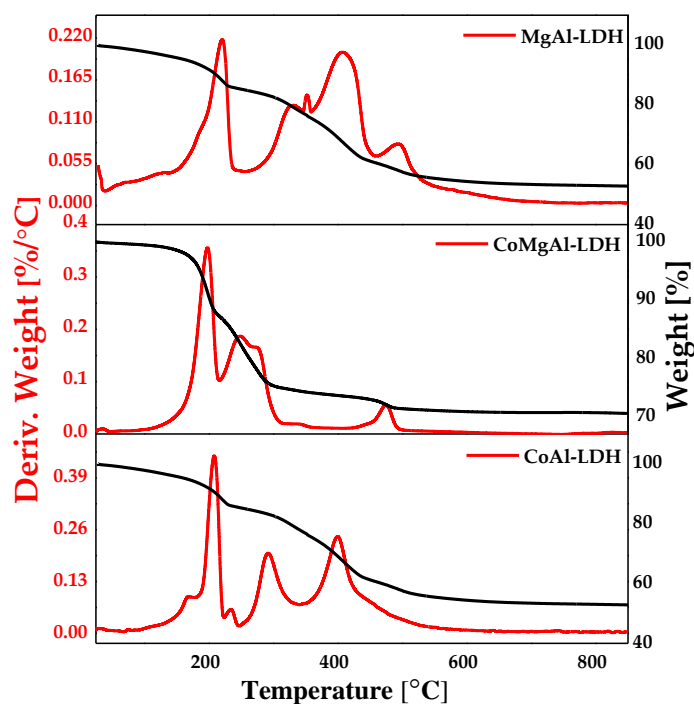


Figure 2. Thermal gravimetric and differential thermal gravimetric analyses of all catalysts.

The thermal behavior of the MgAl-LDH was significantly changed upon the inclusion of cobalt ions in the cationic sheet. The thermal decomposition at lower temperatures was sharply steep, and the Co-Mg-Al LDH sample was recognized as having three main mass loss steps. In the CoAl-LDH sample, the isomorphous substitution of cobalt cations to the magnesium ions in the cationic layer resulted in a similar thermal activity to that of the material MgAl-LDH. The obtained results revealed that the presence of both cobalt and magnesium ions in the cationic sheet favored the thermal decomposition of the catalyst.

2.3. X-ray Diffraction (XRD)

The X-ray powder diffraction pattern of synthetic Mg-Al LDH is shown in Figure 3. A phase analysis showed that only the double layered hydroxide meixnerite phase structure was obtained [40] with chemical formula $Mg_6Al_2(OH)_{18} \cdot 4H_2O$, as indexed by Ref. Pattern 38-0478, JCPDS. Rhombohedral with R-3 m space group was the crystal structure of the investigated MgAl-LDH. The lattice parameters were measured, and the average crystallite sizes from the Scherrer equation were estimated using the basal reflection plane (003) and non-basal line (110) full width at half maximum (FWHM), as used by Mokhtar et al. [17]. The calculated lattice parameter a , which is mainly related to the composition of the cation, was equal to 3.0463 nm. The measured cell parameter c , which is directly linked to the distance between the interlayers, was equivalent to 22.93 nm. The size of crystallite attained was 22 nm. The extended dimension in the c directions was primarily due to the relatively large distance between meixnerite cationic sheets.

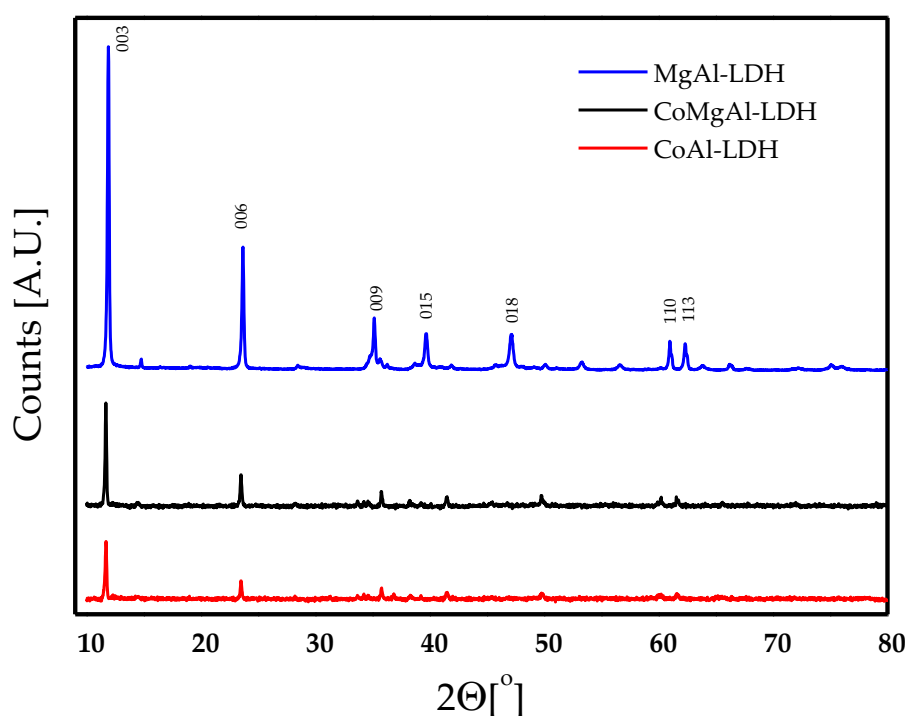


Figure 3. X-ray diffraction (XRD) patterns of all the investigated solid samples.

The CoMgAl-LDH system showed reflections typical of an LDH structure without the appearance of any phase impurities. The stacking of the double hydroxide layers in the BC–CA–AB–BC stacking caused a rhombohedral hydrotalcite-like (meixnerite) structure to form. The relatively sharp XRD reflections for the CoMgAl-LDH catalyst indicate the bigger crystal domain size compared to the MgAl-LDH catalyst. Scherrer analysis of the LDH basal reflection at around $2\theta = 12^\circ$ indicates the apparent crystallite sizes in the c -direction (stacking direction of the LDH sheets) of around 45 nm for the CoMgAl-LDH (Figure 3). CoAl-LDH's XRD pattern indicates the development of a layered double hydroxide phase in three sections: (a) low-angle area ($<30^\circ$ 2θ) covering basal reflections (001); (b,c) far-angle areas ($>55^\circ$ 2θ) comprising the (110) and (113) reflections representative of metal hydroxide layers. The high crystallinity of CoAl-LDH indicates the increase in the crystallite size upon isomorphic substitution of Mg by Co in the cationic sheet. Scherrer analysis of the LDH basal reflection at around $2\theta = 12^\circ$ indicates apparent crystal sizes in the c -direction (stacking direction of the LDH sheets) of around 55 nm.

2.4. Scanning Electron Microscopy and Energy-Dispersive X-ray Spectroscopy (SEM–EDS)

Figure 4 shows SEM images of the as-synthesized (A) MgAl-LDH, (B) CoMgAl-LDH, and (C) CoAl-LDH samples. The morphology of the synthesized layered double hydroxides shows hexagonal platelets with uniform thickness of about 18 nm. The obtained results complement the crystallite size obtained from XRD analysis for pure Mg-Al LDH. The addition of cobalt to the cationic sheet with an isomorphic substitution of magnesium stabilized the hexagonal platelets with a pronounced increase in the platelet thickness (~25 nm) (Figure 4B,C). The hydrothermal preparation method [40] was successful in synthesizing non-sized layered double hydroxide materials of expected high catalytic activity.

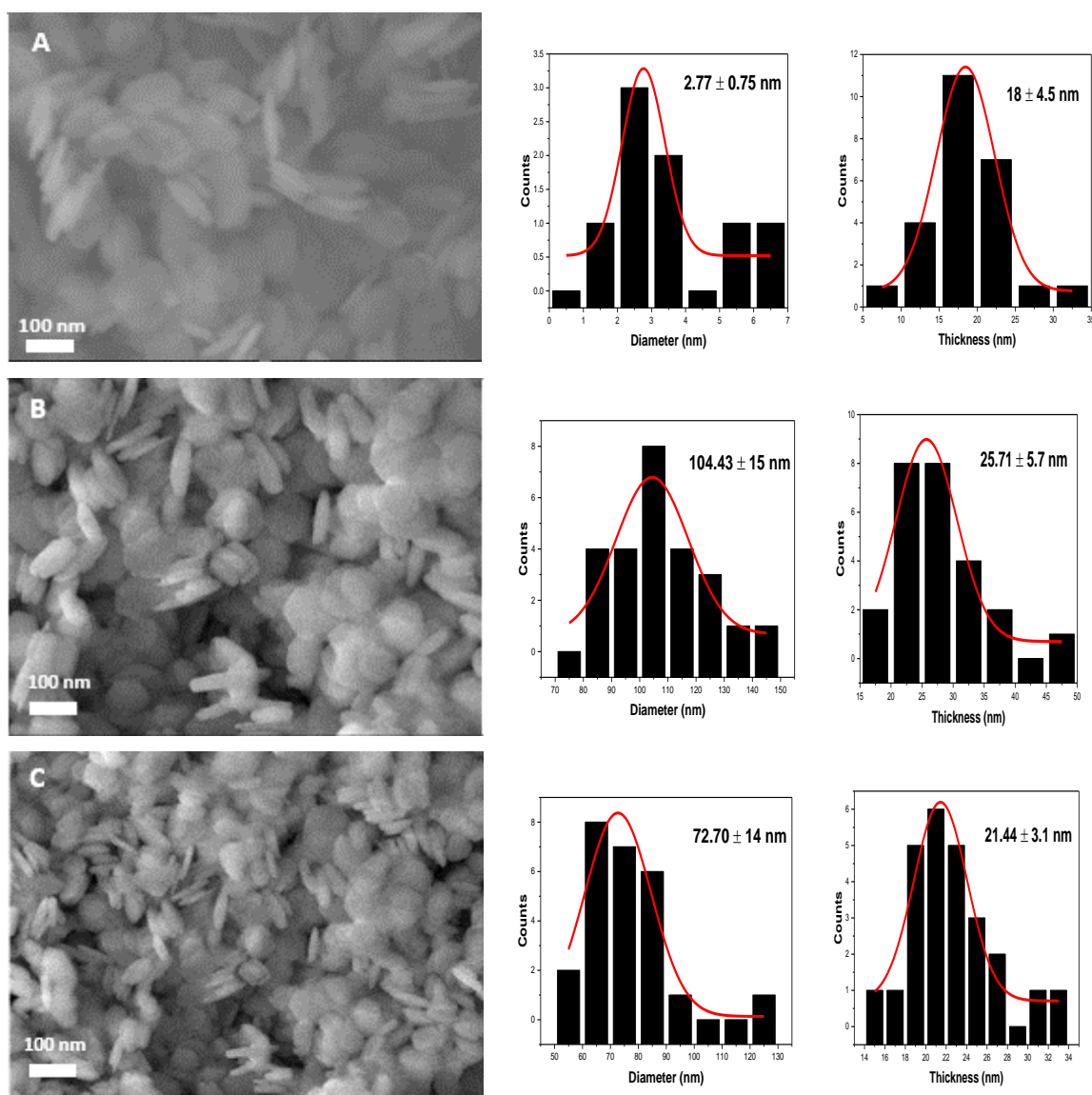


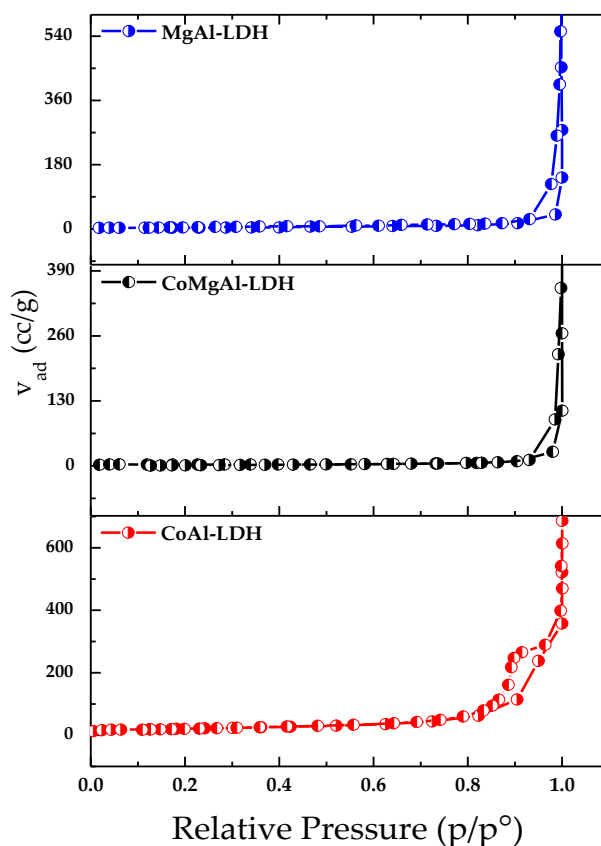
Figure 4. SEM images and particle size distribution analysis for all the investigated samples: (A) MgAl layer double hydroxide (LDH), (B) CoMgAl-LDH, and (C) CoAl-LDH samples. Energy-dispersive spectroscopy (EDS) analyses show pure materials free from any sodium ions with a stoichiometric ratio matching the calculated molar ratios of different cations. EDS analyses confirm the presence of cobalt cations in the chemical structure of the meixnerite phase, detected by XRD analysis. The absence of any diffraction peaks for cobalt compounds in the XRD analysis confirm the uniform isomorphic substitution of magnesium ions by cobalt ions in the cationic sheets (Table 1).

Table 1. Data obtained from EDS analysis for all the investigated samples.

Sample	OK		MgK		AlK		CoK	
	wt.%	at.%	wt.%	at.%	wt.%	at.%	wt.%	at.%
MgAl-LDH	67.47	74.85	25.15	19.44	07.38	05.71	-	-
CoMgAl-LDH	52.95	72.09	10.45	09.36	11.37	09.18	25.23	09.36
CoAl-LDH	50.33	74.64	-	-	11.07	09.74	38.06	15.61

2.5. N₂ Physisorption

Experiments on N₂ adsorption/desorption were performed to analyze the texture characteristics of various investigated LDH products. N₂ isotherms for the adsorption and desorption of examined samples are shown in Figure 5. All the materials displayed a type II isotherm according to International Union for Pure and Applied Chemistry (IUPAC) classification [41] with an H3 hysteresis loop for the entire studied sample except for CoAl-LDH, which showed an H4 hysteresis type. The samples also showed type B behavior, which is typical for clay materials [42]. The BET surface areas, derived from the isotherms for MgAl-LDH, CoMgAl-LDH, and CoAl-LDH samples were 73, 54, and 64 m²/g, respectively. The LDHs with a high anion population in the water layer between sheets, as shown from FTIR spectra for the cobalt-containing LDH samples, showed particle sizes of 24 and 21 nm, for CoMgAl-LDH and CoAl-LDH, respectively. The relatively small surface area values could be attributed to the relatively large particle size and higher anion population, which partially prevented the penetration of N₂ into the pores [43]. The distribution of pores in LDHs is known to be regulated by crystallite size and crystallite packing arrangement [44]. A relatively narrow distribution of pores was observed for MgAl-LDH and CoMgAl-LDH samples, whereas a broader distribution of pores could be observed for the CoAl-LDH sample. This was indeed reflected in the pronounced change in the surface area and the pore nature upon the isomorphic substitution of Mg ions by Co ions in the cationic sheet.

**Figure 5.** N₂ adsorption/desorption isotherms for different investigated materials.

2.6. Temperature-Programmed Desorption (TPD-CO₂)

Michael addition reactions are usually catalyzed using basic catalysts [15]. In the present study, we selected layered double hydroxide-based catalysts as they are well-known basic solid catalysts [39]. The combination of cobalt active species and basicity of the hydrotalcite-like structure could improve the catalytic efficiency of the catalysts toward Michael addition reactions. Therefore, CO₂-TPD was applied to study the basic nature of the synthesized samples. Figure 6 shows the CO₂-TPD profile signals for MgAl-LDH, CoMgAl-LDH, and CoAl-LDH solids. As these catalysts are carbonate-free in the interlayer gallery, the desorption CO₂ peaks are directly related to the adsorbed CO₂ species to the solid surface. It is shown from this figure that MgAl-LDH adsorbed more CO₂ species than the other two samples. The meixnerite phase of MgAl-LDH had terminal hydroxyl groups and more Brønsted basic sites. Therefore, the desorption temperature started at a relatively low temperature (~300 °C). Moreover, the two overlapping peaks with maxima at 330 and 400 °C were assigned as the Brønsted basic sites. The isomorphous partial substitution of cobalt species to the magnesium cations in the cationic sheet did not affect the basic nature of the solid catalyst (CoMgAl-LDH). There was one single sharp peak at 330 °C for CoAl-LDH, as a result of complete substitution of magnesium by cobalt ions in the cationic sheet.

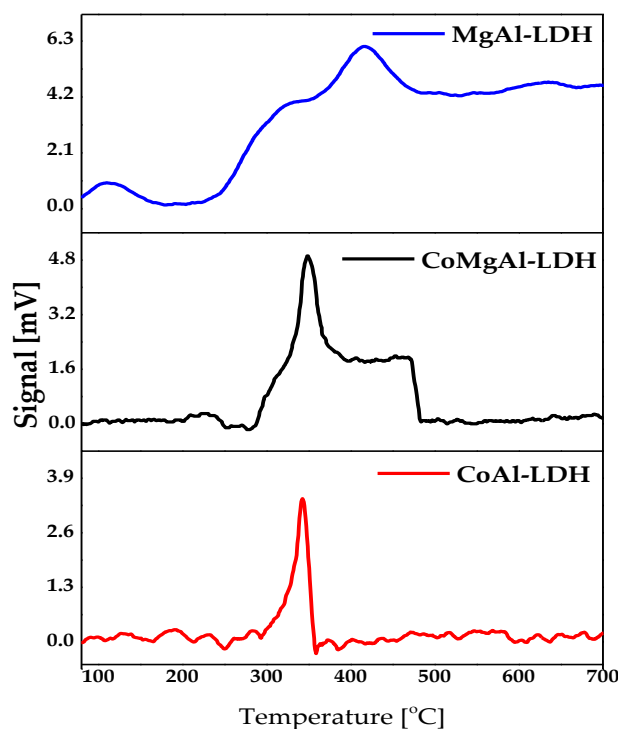
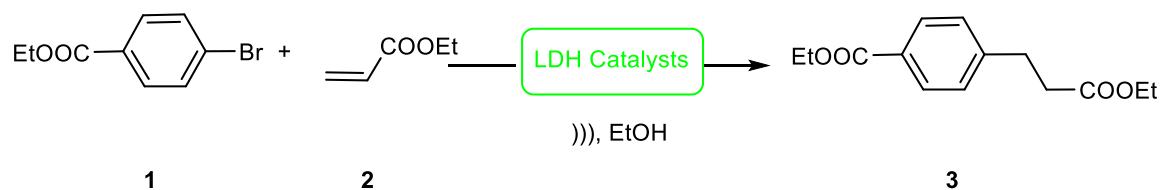


Figure 6. CO₂-TPD profile for all the investigated solid materials.

2.7. Catalytic Test Reaction

The reaction between ethyl *p*-bromobenzoate (1) and ethyl acrylate (2) was investigated through modification of different parameters. The respective conjugate adduct was synthesized in the presence of various synthesized catalysts (Scheme 1).



Scheme 1. Optimizing the reaction conditions.

To improve the reaction conditions, three separate LDH catalysts (0.35 g) were tested using ultrasonic irradiation to react with an equimolar mixture of ethyl *p*-bromobenzoate (1) and ethyl acrylate (2) (Scheme 1). Such solid catalysts, MgAl-LDH, CoMgAl-LDH, and CoAl-LDH, were chosen because they have low environmental impact and are easy to recycle (Table 2).

Table 2. Synthesis of compound 3 using different catalysts under ultrasonic irradiation.

Entry	Catalyst	Conventional Heating		Ultrasonic Irradiation	
		Time (h)	Yield (%)	Time (min)	Yield (%)
1	Catalyst-free	12	-	120	-
2	MgAl-LDH	12	-	120	-
3	CoMgAl-LDH	6	71	45	85
4	CoAl-LDH	8	58	60	72

In order to find the beneficial effect of ultrasound irradiation on the above reaction, we performed the above reaction on the same scale under conventional heating.

From the findings cited in Table 2, it is clear that no substance was formed in the absence of a catalyst under ultrasonic irradiation or traditional conditions, even after 2 h or 12 h, respectively, (entry 1). In addition, the best yield 85% of the desired product 3 was reached using the CoMgAl-LDH catalyst for 45 min. Furthermore, no product was formed using MgAl-LDH under conventional heating or ultrasonic irradiations (entry 2). Introducing cobalt into the cationic sheet of the layered double hydroxide improved the catalytic efficacy of those catalytic materials under classical or ultrasonic irradiation. Utilizing CoMgAl-LDH catalyst resulted in the formation of high yield of the desired product in a short reaction time (entry 3). In contrast, the complete isomorphic substitution of Mg ions by Co ions in the cationic sheet, i.e., in CoAl-LDH, reduced the desired product yield (72%) and increased the reaction time (60 min). Obviously, in the presence of CoMgAl-LDH catalysts, ultrasonic irradiation had a beneficial effect on the formation of the Michael adduct 3 compared to conventional heating, which showed a longer reaction time and lower product yield. To improve the reaction conditions using the best CoMgAl-LDH catalyst, a series of experiments were performed in variable catalyst amounts, and the progress of the reaction was monitored using thin-layer chromatography (TLC) for a typical reaction (Scheme 1) under ultrasonic irradiation. The results obtained from the catalytic test reaction are cited in Table 3.

Table 3. Optimization of reaction condition for synthesis of 3 utilizing CoMgAl-LDH catalyst under ultrasonic irradiation.

Entry	Catalyst Weight (g)	Solvent	Time (min)	Yield (%)
1	0.3	EtOH	45	82
2	0.35	EtOH	45	85
3	0.4	EtOH	45	85
4	0.35	DMF	30	76
5	0.35	Butanol	15	81
6	0.35	Methanol	15	63
7	0.35	Propanol	25	76

Initially, different quantities of the CoMgAl-LDH catalyst were evaluated under the same reaction situations for optimization of the catalyst mass, where the greatest yield was found using 0.35 g of the catalyst with the process running for 45 min (Table 3, entry 2). Moving forward to the investigation of the effect of solvent on this catalytic system, four reactions were performed with DMF, butanol, methanol, and propanol, in addition to ethanol, with the best catalyst amount (entries 2, 4–7). The best solvent for this reaction protocol proved to be EtOH (entry 2), in which the desired product **3** was isolated in 85% yield.

The structure of product **3** was confirmed according to elemental analysis and spectral data. The $^1\text{H-NMR}$ spectrum exhibited two doublets signals at 7.91 and 7.32 due to four aromatic protons, two quartet signals due to two methylene groups of esters at 4.32 and 4.12, two triplet signals at 3.11 and 2.65 due to two adjacent methylene groups, and two triplets at 1.39 and 1.29 due to two methyl groups of esters. This spectroscopic data of the reaction product and the satisfactory elemental analysis supported the structure ethyl 4-(3-ethoxy-3-oxopropyl)benzoate **3**.

Under optimized reaction conditions, the reusability of the CoMgAl-LDH catalyst was tested for several reaction cycles for synthesis of compound **3** (Figure 7), where the catalyst was washed with hot ethanol and dried under vacuum after completion of the reaction. Using the same reaction conditions, the recuperated catalyst was reused five times. Figure 6 shows that, even after being used up to five times, the regenerated catalyst conducted the reactions effectively under the same conditions. The slight decay observed at the fourth and fifth repeats in the catalytic activity of the CoMgAl-LDH catalyst could be attributed to the catalyst's weight loss.

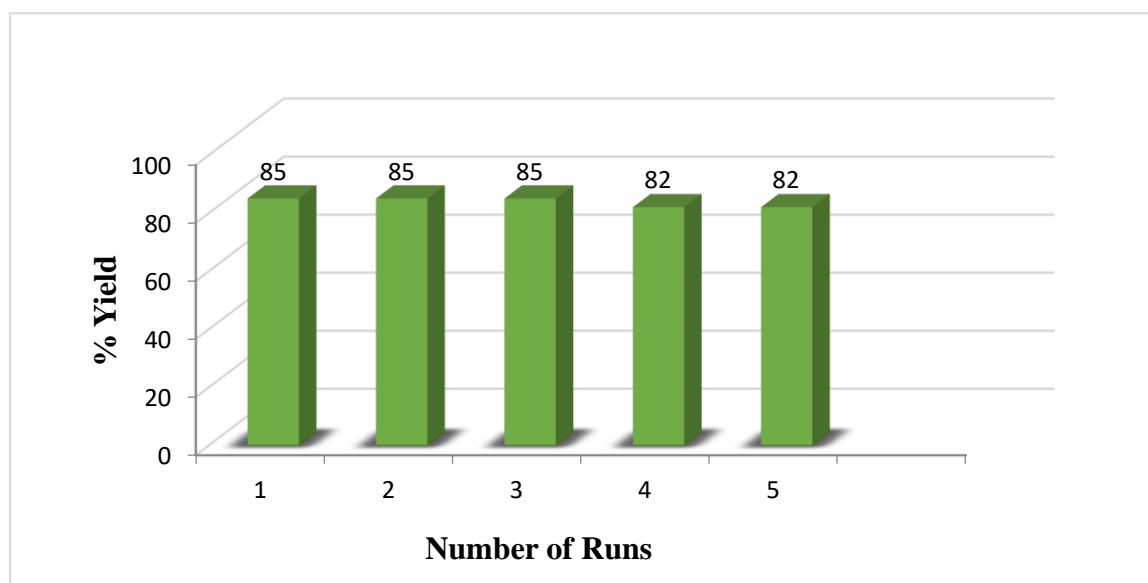
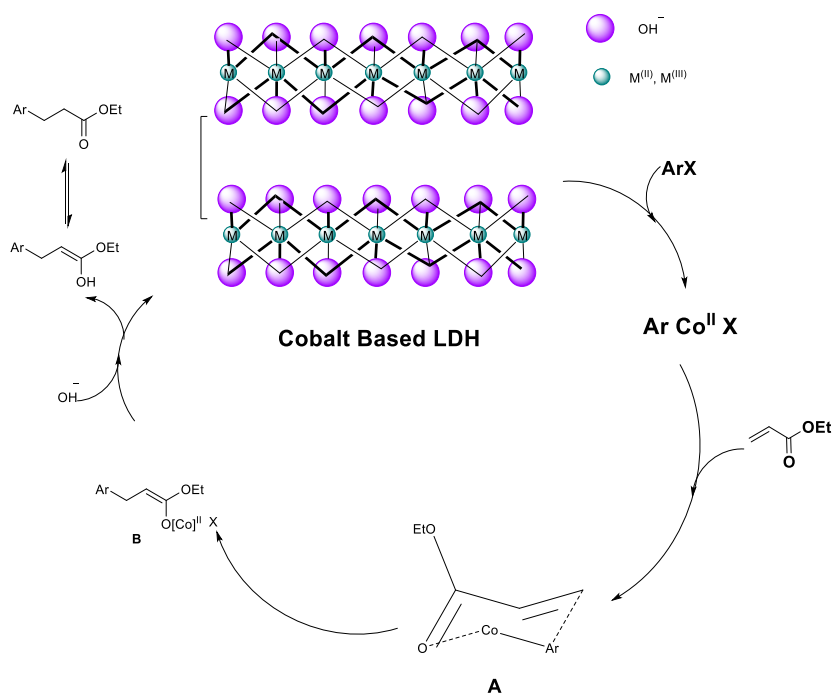


Figure 7. Re-usability of CoMgAl-LDH catalyst for formation of compound **3**.

It is obvious, in the light of the above findings, that the addition of cobalt to MgAl-LDH had a key role for this reaction. The mechanism for this reaction was, therefore, postulated, in which low-valent cobalt species are most likely to develop with an aryl halide via oxidative addition to form an aryl-cobalt intermediate that could react via nucleophilic attack in a six-member transition state [A] with electron-deficient olefin, leading to an intermediate cobalt enolate [B] [45] (Scheme 2). The latter species reacts with the basic catalytic site to restore the expected 1,4-adduct release of the Co^{II} species to the catalyst.



Scheme 2. Suggested mechanism for the conjugate addition reaction.

Noteworthy, the higher catalytic efficacy and the accountable yield of the anticipated products were due to different parameters in a short reaction time: (i) the physicochemical characteristics of the catalyst, i.e., their chemical, structural, permeable, and basic characteristics; (ii) reaction conditions, i.e., ultrasonic irradiation. Introducing cobalt to the cationic sheet improved the catalytic efficiency of the cobalt-containing catalysts. However, this superior activity was reduced upon complete substitution of magnesium cations by cobalt cations in the cationic sheet, i.e., CoAl-LDH catalyst. These results revealed the synergistic effect between cobalt and the basic nature of meixnerite phase in tuning the catalytic efficiency of the Co-containing layered double hydroxide catalyst in conjugate addition of functionalized aryl compounds into Michael acceptors. The results of physicochemical analyses and crystallography clearly display that the Co-treatment samples maintained a crystalline structure as the isomorphic substitution of Mg^{2+} ions by Co^{2+} ions occurred. The partial substitution of the basic Mg^{2+} cations in the cationic sheet by other cations such as Co^{2+} cations affected the thermal behavior of the CoMgAl-LDH catalyst, as seen from TGA data. The synergistic effect between the Co^{2+} ions and the basic component played a role in the catalytic activity. Moreover, ultrasound irradiation had a beneficial effect on the reaction in the presence of the CoMgAl-LDH catalyst, lowering the reaction time and increasing the product yield. This obvious effect can be reasonably interpreted in terms of the physical phenomenon known as acoustic cavitation (at the solid/liquid interface) [46,47]. It was suggested that the micro-jet impact and shockwave damage on the surface of the solid (catalyst), along with the shock wave associated with the cavitation collapse, would cause localized deformation and surface erosion, which would increase the size of the possible reaction area [47].

3. Materials and Methods

3.1. Materials

Chemical reagents used in this work included sodium hydroxide solution (Fluka AG, Chemische Fabrik CH-9470 Buchs, Switzerland), aluminum nitrate nonahydrate (PRS, Panreac Química SLU, Barcelona, Spain), magnesium nitrate hexahydrate, cobalt(II) nitrate hexahydrate, and sodium carbonate (BDH Chemical Ltd., Dubai, UAE). All organic solvents were purchased from (Fluka AG, Chemische Fabrik CH-9470 Buchs, Switzerland) and used as received unless otherwise stated.

3.2. Preparation of Catalysts

All catalytic samples were prepared using a coprecipitation method followed by post-hydrothermal treatment under autogenous pressure. Three different solutions containing nitrate salts Mg/Al ratio of 3:1, Co/Mg/Al ratio of 1.5:1.5:1, and Co/Al ratio of 3:1 were dissolved in deionized water (250 mL) to give a solution concentration of 1 M, and this solution was denoted as solution A. Another solution denoted solution B was prepared using NaOH and Na₂CO₃ dissolved in deionized water (250 mL) to give a solution concentration of 1 M. Solutions A and B were added simultaneously to form the mixed base solution (as precipitating agent) at 30 °C and pH = 11 under N₂ atmosphere. All precipitates were aged overnight prior to transferring them to an autoclave and hydrothermally treating them at 170 °C for 24 h. The cake was centrifuged and then dried at 100 °C for 16 h. The synthesized solids were named MgAl-LDH, CoMgAl-LDH, and CoAl-LDH.

3.3. Measurements and Characterization

FTIR spectrometer (PerkinElmer) was used to perform Fourier-infrared transfer (FTIR) spectroscopy in transmission mode. The measurements were carried out in the wavenumber range 4000–400 cm⁻¹ with 4-cm⁻¹ resolution.

Thermogravimetric analysis (TGA) runs on a TA TGA-Q500 model were carried out. In each cycle, 6–10 mg was put in the TGA pan and heated to 800 °C at 10 °C·min⁻¹ in N₂ atmosphere (40 mL·min⁻¹ flow rate).

Measurements for powder X-ray diffraction (PXRD) were carried out at room temperature using a Bruker diffractometer (Bruker D8 advance target, Karlsruhe, Germany). The patterns were collected using Cu Kα1 radiation and a 40 kV and 40 mA monochromator ($\lambda = 1.5405 \text{ \AA}$), with 2θ varying between 2° and 80°. X'Pert HighScore Plus software was used to analyze the spectra. The crystallite size of Ni-LDH was calculated using the Scherrer equation.

$$d \text{ (nm)} = \frac{0.9 \times \lambda}{B \times \cos(\theta)}$$

where d is the mean Ni-LDH crystallite size under investigation, λ is wavelength of the X-ray beam used, 0.9 is the Scherrer constant, B is the full width at half maximum (FWHM) of the diffraction peak, and θ is the diffraction angle.

High-resolution field-emission (FEG quanta 250) scanning electron microscopy (SEM) allowed the chemistry of materials to be investigated on the sub-micron scale.

The texture properties of the prepared samples were calculated from nitrogen adsorption/desorption isothermal measurements at 77 K using the automated gas sorption device NOVA3200e (Quantachrome, Boynton Beach, FL, USA) model. Every sample was degassed at 100 °C for 12 h prior to the measurement. The actual surface area, S_{BET} , was determined using the Brunauer–Emmett–Teller (BET) equation [48]. The distribution of the pore size over the mesopore range was generated by Barrett–Joyner–Halenda (BJH) [49] analysis of the desorption branches, and mean pore size values were estimated.

Measurements of carbon dioxide temperature-programmed desorption (TPD-CO₂) were carried out using CHEMBET 3000 (Quantachrome, FL, USA). A sample exhaust at 100 °C (1 h) was performed when helium was transferred to physical water detachment. The sample's CO₂ saturation then occurred at 120 °C. The temperature-programmed desorption was easily achieved by ramping the adsorbent temperature to 800 °C at 10 °C/min.

Thin-layer chromatography (TLC) was performed on precoated Merck 60 GF254 silica gel plates with a fluorescent indicator and UV light detection at 254 and 360 nm. The melting points of the organic materials were determined on a Stuart melting point apparatus and were not corrected.

IR spectra were recorded on the Smart iTR, an ultra-high-performance, flexible attenuated total reflectance (ATR) sampling system on the Nicolet iS10 FT-IR spectrometer.

The NMR spectra were registered on a Bruker Avance III 400 spectrometer (9.4 T, 400.13 MHz for ^1H and 100.62 MHz for ^{13}C) with a 5-mm BBFO probe at 298 K. Chemical changes (δ in ppm) are given in relation to the internal solvent, DMSO; 2.50 was used as an external norm for ^1H and 39.50 was used for ^{13}C . Mass spectra were recorded on a single-quadrupole GC–MS Thermo ISQ. Elemental analyses were performed for C, H, N, and S on an EA3000 Series EuroVector instrument. Ultrasonic irradiation experiments were carried out using an ultrasonic cleaning bath Elma P30H.

3.4. Typical Procedure for Conjugate Addition Reaction

3.4.1. Conventional Condition

To a stirred solution of 25 mL of ethanol, an equimolar amount of ethyl *p*-bromobenzoate (**1**) and ethyl acrylate (**2**) was added, followed by 0.35 g of LDH catalyst 80 °C. The reaction progress was monitored by thin-layer chromatography until the aryl halide was consumed. The mixture was filtrated to separate the catalyst, and the filtrate was evaporated to get a yellow oil which was purified by column chromatography on a silica gel (pentane/diethylether) to afford the conjugate adduct **3** in pure form.

3.4.2. Ultrasonic Condition

The reaction here was done on the same scale as described in above conventional condition, whereby a round-bottom flask was placed in the cleaning bath.

The spectroscopic data of compound **3** are as follows:

IR (ν_{\max} , cm^{-1}) 2980, 1713, 1611, 1272; $^1\text{H-NMR}$ (400 MHz, DMSO) δ 7.98 (d, $J = 8.3$ Hz, 2H), 7.28 (d, $J = 8.3$ Hz, 2H), 4.37 (q, $J = 7.1$ Hz, 2H), 4.13 (q, $J = 7.1$ Hz, 2H), 3.01 (t, $J = 7.7$ Hz, 2H), 2.65 (t, $J = 7.7$ Hz, 2H), 1.39 (t, $J = 7.1$ Hz, 3H), 1.24 (t, $J = 7.1$ Hz, 3H); $^{13}\text{C-NMR}$ (100 MHz, DMSO) δ 172.6, 166.6, 145.9, 129.8 (2C), 128.6, 128.3 (2C), 60.9, 60.6, 35.4, 30.9, 14.3, 14.2; ESI-MS m/z (relative intensity) 250 (M^+).

4. Conclusions

Coprecipitation under inert atmosphere followed by hydrothermal treatment under autogenous pressure was a successful tool for the preparation of hydrotalcite-like materials (meixnerite). Partial isomorphous substitution of magnesium by cobalt in the cationic sheet of a layered double hydroxide resulted in the formation of a catalyst for the coupling of ethyl *p*-bromobenzoate with ethyl acrylate. This catalytic method uses a simple CoMgAl-LDH, which tends to be an extremely suitable catalyst for a wide variety of substrates ranging from aryl halides to many reactive groups. The reaction affords excellent yields in a rapid reaction period under ultrasound irradiation. The superior catalytic efficiency was allocated to the synergistic effect between Co ions in the cationic sheet and the basicity of the layered materials.

Author Contributions: M.M. conceptualized and designed the experiments; N.S.A. performed the experiments; F.M.A.-N. analyzed the data; T.S.S. contributed reagents/materials/analysis tools; M.M. wrote the paper. All authors edited and revised the manuscript before submission. All authors have read and agreed to the published version of the manuscript.

Funding: This research received no external funding.

Acknowledgments: The authors acknowledge Huda Sherbini and Ghalia Alzahrani for their contribution to TPD measurements. The group of surface chemistry and catalytic studies in the Chemistry Department, Faculty of Science, KAU, is acknowledged for the facilities provided to carry out this research.

Conflicts of Interest: The authors declare no conflicts of interest.

References

1. Perlmutter, P. *Conjugate Addition Reactions in Organic Synthesis*, 1st ed.; Pergamon Press: Oxford, UK, 1992.

- Muriel, A.; Gosmini, C.; Périchon, J. CoBr₂(Bpy): An Efficient Catalyst for the Direct Conjugate Addition of Aryl Halides or Triflates onto Activated Olefins. *J. Org. Chem.* **2006**, *71*, 6130–6134.
- Tucker, C.E.; Majid, T.N.; Knochel, P. Preparation of highly functionalized magnesium, zinc, and copper aryl and alkenyl organometallics via the corresponding organolithiums. *J. Am. Chem. Soc.* **1992**, *114*, 3983–3985. [[CrossRef](#)]
- Varchi, G.; Ricci, A.; Cahiez, G.; Knochel, P. Copper Catalyzed Conjugate Addition of Highly Functionalized Arylmagnesium Compounds to Enones. *Tetrahedron* **2000**, *56*, 2727–2731. [[CrossRef](#)]
- Klement, I.; Stadtmüller, H.; Knochel, P.; Cahiez, G. Preparation and reactivity of functionalized aryl and alkenylmanganese halides. *Tetrahedron Lett.* **1997**, *38*, 1927–1930. [[CrossRef](#)]
- Lu, X.; Lin, S. Pd(II)-Bipyridine Catalyzed Conjugate Addition of Arylboronic Acid to α,β -Unsaturated Carbonyl Compounds. *J. Org. Chem.* **2005**, *70*, 9651–9653. [[CrossRef](#)] [[PubMed](#)]
- Liu, R.; Yang, Z.; Ni, Y.; Song, K.; Shen, K.; Lin, S.; Pan, Q. Pd(II)/Bipyridine-Catalyzed Conjugate Addition of Arylboronic Acids to α,β -Unsaturated Carboxylic Acids. Synthesis of β -Quaternary Carbons Substituted Carboxylic Acids. *J. Org. Chem.* **2017**, *82*, 8023–8030. [[CrossRef](#)] [[PubMed](#)]
- Vautravers, N.R.; Breit, B. Rhodium(I)-Catalyzed 1,4-Addition of Arylboronic Acids to Acrylic Acid in Water: One-Step Preparation of 3-Arylpropionic Acids. *Synlett* **2011**, *17*, 2517–2520. [[CrossRef](#)]
- Kamikawa, K.; Tseng, Y.-Y.; Jian, J.-H.; Takahashi, T.; Ogasawara, M. Planar-Chiral Phosphine-Olefin Ligands Exploiting a (Cyclopentadienyl)manganese(I) Scaffold to Achieve High Robustness and High Enantioselectivity. *J. Am. Chem. Soc.* **2017**, *139*, 1545–1553. [[CrossRef](#)] [[PubMed](#)]
- Wu, C.; Yue, G.; Nielsen, C.D.-T.; Xu, K.; Hirao, H.; Zhou, J. Asymmetric Conjugate Addition of Organoboron Reagents to Common Enones Using Copper Catalysts. *J. Am. Chem. Soc.* **2016**, *138*, 742–745. [[CrossRef](#)] [[PubMed](#)]
- Lerebours, R.; Wolf, C. Palladium(II)-Catalyzed Conjugate Addition of Arylsiloxanes in Water. *Org. Lett.* **2007**, *9*, 2737–2740. [[CrossRef](#)] [[PubMed](#)]
- Westermann, J.; Imberg, U.; Nguyen, A.T.; Nickisch, K. Nickel-Catalysed 1,4-Addition of Aryl Groups to Enones Using Aryldialkylaluminum Compounds. *Eur. J. Inorg. Chem.* **1998**, *295*, 295–298. [[CrossRef](#)]
- Subburaj, K.; Montgomery, J. A New Catalytic Conjugate Addition/Aldol Strategy That Avoids Preformed Metalated Nucleophiles. *J. Am. Chem. Soc.* **2003**, *125*, 11210–11211. [[CrossRef](#)] [[PubMed](#)]
- Gomes, P.; Gosmini, C.; Nédélec, J.Y.; Périchon, J. Electrochemical vinylation of aryl and vinyl halides with acrylate esters catalyzed by cobalt bromide. *Tetrahedron Lett.* **2002**, *43*, 5901–5903. [[CrossRef](#)]
- Amatore, M.; Gosmini, C.; Périchon, J. Process for Forming Carbon-Carbon Bonds by a Coupling Reaction between Unsaturated Compounds in the Presence of a Cobalt-Based Catalyst. Centre National de la Recherche Scientifique CNRS Rhodia Chimie SAS. Patent FR2865203, 22 July 2005.
- Ahmed, N.S.; Menzel, R.; Wang, Y.; Garcia-Gallastegui, A.; Bawaked, S.M.; Obaid, A.Y.; Basahel, S.N.; Mokhtar, M. Graphene-oxide-supported CuAl and CoAl layered double hydroxides as enhanced catalysts for carbon-carbon coupling via Ullmann reaction. *J. Solid State Chem.* **2017**, *246*, 130–137. [[CrossRef](#)]
- Mokhtar, M.; Inayat, A.; Ofili, J.; Schwieger, W. Thermal decomposition, gas phase hydration and liquid phase reconstruction in the system Mg/Al hydrotalcite/mixed oxide: A comparative study. *Appl. Clay Sci.* **2010**, *50*, 176–181. [[CrossRef](#)]
- Mokhtar, M.; Saleh, T.S.; Ahmed, N.S.; Al-Thabaiti, S.A.; Al-Shareef, R.A. An eco-friendly N-sulfonylation of amines using stable and reusable Zn–Al–hydrotalcite solid base catalyst under ultrasound irradiation. *Ultrason. Sonochem.* **2011**, *18*, 172–176. [[CrossRef](#)] [[PubMed](#)]
- Mokhtar, M.; Saleh, T.S.; Basahel, S.N. Mg–Al hydrotalcites as efficient catalysts for aza-Michael addition reaction: A green protocol. *J. Mol. Catal. A Chem.* **2012**, *353–354*, 122–131. [[CrossRef](#)]
- Narasimharao, K.; Al-Sabban, E.; Saleh, S.T.; Garcia-Gallastegui, A.; Sanfiz, A.C.; Basahel, S.; Al-Thabaiti, S.; Alyoubi, A.; Obaid, A.; Mokhtar, M. Microwave assisted efficient protocol for the classic Ullmann homocoupling reaction using Cu–Mg–Al hydrotalcite catalysts. *J. Mol. Catal. A Chem.* **2013**, *379*, 152–162. [[CrossRef](#)]
- Abdellattif, M.; Mokhtar, H.M. MgAl-Layered Double Hydroxide Solid Base Catalysts for Henry Reaction: A Green Protocol. *Catalysts* **2018**, *8*, 133. [[CrossRef](#)]
- Alzhrani, G.; Ahmed, N.S.; Aazam, E.S.; Saleh, T.S.; Mokhtar, M. Novel Efficient Pd-Free Ni-Layered Double Hydroxide Catalysts for a Suzuki C–C Coupling Reaction. *Chem. Select* **2019**, *4*, 7904–7911. [[CrossRef](#)]

23. Abbasi, A.R.; Akhbari, K.; Morsali, A. Dense coating of surface mounted CuBTC metal–organic framework nanostructures on silk fibers, prepared by layer-by-layer method under ultrasound irradiation with antibacterial activity. *Ultrason. Sonochem.* **2012**, *19*, 846–852. [[CrossRef](#)] [[PubMed](#)]
24. Safarifard, V.; Morsali, A. Applications of ultrasound to the synthesis of nanoscale metal–organic coordination polymers. *Coord. Chem. Rev.* **2015**, *292*, 1–14. [[CrossRef](#)]
25. Li, Z.-Q.; Qiu, L.-G.; Wang, W.; Xu, T.; Wu, Y.; Jiang, X. Fabrication of nanosheets of a fluorescent metal–organic framework [Zn(BDC)(H₂O)]_n (BDC= 1,4-benzenedicarboxylate): Ultrasonic synthesis and sensing of ethylamine. *Inorg. Chem. Commun.* **2008**, *11*, 1375–1377. [[CrossRef](#)]
26. Abdollahi, N.; Masoomi, M.Y.; Morsali, A.; Junk, P.C.; Wang, J. Sonochemical synthesis and structural characterization of a new Zn(II) nanoplate metal–organic framework with removal efficiency of Sudan red and Congo red. *Ultrason. Sonochem.* **2018**, *45*, 50–56. [[CrossRef](#)] [[PubMed](#)]
27. Eghbali-Arani, M.; Sobhani-Nasab, A.; Rahimi-Nasrabadi, M.; Ahmadi, F.; Pourmasoud, S. Ultrasound-assisted synthesis of YbVO₄ nanostructure and YbVO₄/CuWO₄ nanocomposites for 20 enhanced photocatalytic degradation of organic dyes under visible light. *Ultrason. Sonochem.* **2018**, *43*, 120–135. [[CrossRef](#)]
28. Choudhary, B.M.; Lakshmi, K.M.; Neeraja, V.; Koteswara, R.K.; Figueras, F.; Delmotte, L. Layered double hydroxide fluoride: A novel solid base catalyst for C–C bond formation. *Green Chem.* **2001**, *3*, 257–260. [[CrossRef](#)]
29. Kantam, M.L.; Ravindra, A.; Reddy, C.V.; Sreedhar, B.; Choudary, B.M. Layered Double Hydroxides-Supported Diisopropylamide: Synthesis, Characterization and Application in Organic Reactions. *Adv. Synth. Catal.* **2006**, *348*, 569–578. [[CrossRef](#)]
30. Varga, G.; Kozma, V.; Kolcsár, V.J.; Kukovecz, Á.; Kónya, Z.; Sipos, P.; Szöllösi, G. β-Isocupreidinate-CaAl-layered double hydroxide composites—Heterogenized catalysts for asymmetric Michael addition. *Mol. Catal.* **2019**, *482*, 110675. [[CrossRef](#)]
31. El-bendary, M.M.; Saleh, T.S.; Al-Bogami, A.S. Ultrasound Assisted High-Throughput Synthesis of 1,2,3-Triazoles Libraries: A New Strategy for “Click” Copper-Catalyzed Azide-Alkyne Cycloaddition Using Copper(I/II) as a Catalyst. *Catal. Lett.* **2018**, *148*, 3797–3810. [[CrossRef](#)]
32. Al-Bogami, A.S.; Saleh, T.S.; Moussa, T.A.A. Green synthesis, antimicrobial activity and cytotoxicity of novel fused pyrimidine derivatives possessing a trifluoromethyl moiety. *Chemistryselect* **2018**, *3*, 8306–8311. [[CrossRef](#)]
33. Saleh, T.S.; Narasimharao, K.; Ahmed, N.S.; Basahel, S.N.; Al-Thabaiti, S.A.; Mokhtar, M. Mg–Al hydrotalcite as an efficient catalyst for microwave assisted regioselective 1,3-dipolar cycloaddition of nitrilimines with the enaminone derivatives: A green protocol. *J. Mol. Catal. A Chem.* **2013**, *367*, 12–22. [[CrossRef](#)]
34. Mokhtar, M.; Saleh, T.S.; Ahmed, N.S.; Al-Bogami, A.S. A Green Mechanochemical One-Pot Three-Component Domino Reaction Synthesis of Polysubstituted Azoloazines Containing Benzofuran Moiety: Cytotoxic Activity against HePG2 Cell Lines. *Polycycl. Aromat. Compd.* **2018**, 1–15.
35. Béres, A.; Palinko, I.; Kiricsi, I.; Nagy, J.B.; Kiyozumi, Y.; Mizukami, F. Layered double hydroxides and their pillared derivatives—Materials for solid base catalysis; synthesis and characterization. *Appl. Catal. A* **1999**, *182*, 237–247. [[CrossRef](#)]
36. Velu, S.; Shah, N.; Jyothi, T.M.; Sivasanker, S. Effect of manganese substitution on the physicochemical properties and catalytic toluene oxidation activities of Mg–Al layered double hydroxides. *Microporous Mesoporous Mater.* **1999**, *33*, 61–75.
37. Di Cosimo, J.I.; Díez, V.K.; Xu, M.; Iglesia, E.; Apesteguía, C.R. Structure and surface and catalytic properties of Mg–Al basic oxides. *J. Catal.* **1998**, *178*, 499–510. [[CrossRef](#)]
38. Tichit, D.; Naciri Bennani, M.; Figueras, F.; Ruiz, J.R. Decomposition processes and characterization of the surface basicity of Cl⁻ and CO₃²⁻ hydrotalcites. *Langmuir* **1998**, *14*, 2086–2091. [[CrossRef](#)]
39. Rocha, J.; del Arco, M.; Rives, V.; Ulibarri, M.A. Reconstruction of layered double hydroxides from calcined precursors: A powder XRD and ²⁷Al MAS NMR study. *J. Mater. Chem.* **1999**, *9*, 2499–2503. [[CrossRef](#)]
40. Liao, H.; Jia, Y.; Wang, L.; Yin, Q.; Han, J.; Sun, X.; Wei, M. Size Effect of Layered Double Hydroxide Platelets on the Crystallization Behavior of Isotactic Polypropylene. *ACS Omega* **2017**, *2*, 4253–4260.
41. Sing, K.S.W.; Everett, D.H.; Haul, R.A.W.; Moscou, L.; Pierotti, R.A.; Rouquérol, J.; Siemieniewska, T. Reporting physisorption data for gas/solid systems with special reference to the determination of surface area and porosity. *Pure Appl. Chem.* **1985**, *57*, 603–619. [[CrossRef](#)]

42. Bergada, O.; Vicente, I.; Salagre, P.; Cesteros, Y.; Medina, F.; Sueiras, J.E. Microwave effect during aging on the porosity and basic properties of hydrotalcites. *Microporous Mesoporous Mater.* **2007**, *101*, 363–373. [[CrossRef](#)]
43. Lowell, S.; Shields, J.E.; Thomas, M.A.; Thommes, M. *Characterization of Porous Solids and Powders: Surface Area, Pore Size and Density*; Kluwer Academic Publishers: Dordrecht, The Netherlands, 2004.
44. Prinetto, F.; Ghiotti, G.; Graffin, P.; Tichit, D. Synthesis and characterization of sol-gel Mg/Al and Ni/Al layered double hydroxides and comparison with co-precipitated samples. *Microporous Mesoporous Mater.* **2000**, *39*, 229–247. [[CrossRef](#)]
45. Amatore, M.; Gosmini, C.; Pe´richon, J. Cobalt-Catalyzed Vinylation of Functionalized Aryl Halides with Vinyl Acetates. *J. Eur. J. Org. Chem.* **2005**, *2005*, 989–992. [[CrossRef](#)]
46. Mason, T.J.; Tiehm, A. *Advances in Sonochemistry: Ultrasound in Environmental Protection*, 1st ed.; Elsevier: Amsterdam, The Netherlands, 2001.
47. Shah, Y.T.; Pandit, A.B.; Moholkar, V.S. *Cavitation Reaction Engineering*, 1st ed.; Springer Science & Business Media, LLC: New York, NY, USA, 1999.
48. Brunauer, S.; Emmett, P.H.; Teller, E. Adsorption of Gases in Multimolecular Layers. *J. Am. Chem. Soc.* **1938**, *60*, 309–319. [[CrossRef](#)]
49. Barrett, E.P.; Joyner, L.G.; Halenda, P.P. The Determination of Pore Volume and Area Distributions in Porous Substances. I. Computations from Nitrogen Isotherms. *J. Am. Chem. Soc.* **1951**, *73*, 373–380. [[CrossRef](#)]



© 2020 by the authors. Licensee MDPI, Basel, Switzerland. This article is an open access article distributed under the terms and conditions of the Creative Commons Attribution (CC BY) license (<http://creativecommons.org/licenses/by/4.0/>).